Theory of Ion and Water Transport in Reverse-Osmosis Membranes

Y. S. Oren and P. M. Biesheuvel
Wetsus, European Centre of Excellence for Sustainable Water Technology, Oostergoweg 9, 8911 MA Leeuwarden, The Netherlands

(Received 26 June 2017; revised manuscript received 23 November 2017; published 28 February 2018)

We present a theory for ion and water transport through reverse-osmosis (RO) membranes based on a Maxwell-Stefan framework combined with hydrodynamic theory for the reduced motion of particles in thin pores. We take into account all driving forces and frictions both on the fluid (water) and on the ions including ion-fluid friction and ion-wall friction. By including the acid-base characteristic of the carbonic acid system, the boric acid system, H_3O^+/OH^-, and the membrane charge, we locally determine pH, the effective charge of the membrane, and the dissociation degree of carbonic acid and boric acid. We present calculation results for an experiment with fixed feed concentration, where effluent composition is a self-consistent function of fluxes through the membrane. A comparison with experimental results from literature for fluid flow vs pressure, and for salt and boron rejection, shows that our theory agrees very well with the available data. Our model is based on realistic assumptions for the effective size of the ions and makes use of a typical pore size of a commercial RO membrane.

DOI: 10.1103/PhysRevApplied.9.024034

I. INTRODUCTION

Reverse osmosis (RO) is one of the main technologies to produce potable water by the desalination of seawater and brackish water, and its application is expected to further increase over the coming years [1,2]. The principle of RO is to apply high pressure on an aqueous solution in contact with a membrane that allows the passage of water but hinders the transport of salt. If the pressure is high enough to overcome the osmotic pressure of the solution, water will pass the membrane, resulting in a low-in-salt permeate stream. The possibility to desalinate water by the RO principle was already shown in the 1850s [3], but it was not until the 1960s when cellulose acetate membranes were introduced that RO gained real industrial potential for the production of desalinated water. Still, there were many issues to be solved in order to make RO commercially competitive and ultimately to become the preferred technology. One of the major issues at that time was the high energy consumption required to operate an RO desalination plant. Since the osmotic pressure of seawater is about 30 bar, the pressure that has to be applied to overcome the osmotic pressure is "lost" with the brine. In the 1980s, energy-recovery devices for RO were introduced to recover this potential energy of the brine. Together with the introduction of thin-film composite (TFC) polyamide (PA) membranes that increased permeate flux and improved rejection [4], RO energy consumption decreased dramatically over the years to values that nowadays are only 2 or 3 times above thermodynamic minimum, making RO currently the most energy-efficient desalination method [5]. In addition to the production of water for human consumption and agriculture, RO is used in many industries for the production and processing of food, pharmaceuticals, textile, and paper [6].

While there has been immense progress in RO development over the past decades, the mechanism of transport and separation in RO membranes is not yet fully understood [7–9]. To describe the physical-chemical phenomena that govern ion and water transport in RO membranes, various mathematical models were developed over the years. Among these models are (1) the solution-diffusion model, which assumes that pressure and concentration gradients are the driving forces for the RO process, (2) pore-flow models based on the pressure difference as the driving force, and (3) molecular dynamics simulations that address the molecular level, thereby taking membrane composition into account. In addition, models based on irreversible thermodynamics use a phenomenological approach to describe membrane transport [6,10,11].

In the present work, we aim to describe the mechanisms by which ions are transported in RO membranes with a Maxwell-Stefan approach combined with information from hydrodynamic theory of particles in thin pores. We restrict our model to the very thin PA layer in a TFC membrane and the concentration-polarization layer located in front of the membrane, and focus on the desalination of artificial seawater. We study the effect of applied pressure and membrane charge on the composition of the permeate, such as salt concentration and pH, and compare with literature values.

II. THEORETICAL BACKGROUND

A. RO membranes

Since development of RO membranes for seawater desalination started in the 1960s, much progress has been made. The first membranes were made of cellulose acetate (CA) with the most significant improvement made by Loeb and Sourirajan [12]. Their asymmetric membrane, a 200-nm CA film on top of a porous support, laid the foundation for industrial-scale seawater desalination by RO [13]. Although the CA membranes allowed for at least an order of magnitude higher water flux than other membranes available at the time, these membranes were not durable when exposed to *p*H changes, chlorine, and microbial contamination. Since then, many types and forms of RO membranes have been developed. Today the most common RO membrane used in commercial installations is a TFC membrane with a PA top layer. This material was introduced in the 1970s [14] and provides better performance than CA membranes in terms of flux, salt rejection, *p*H tolerance, and the range of temperatures it can withstand [14,15]. These membranes consist of a very thin layer of aromatic PA (50–150 nm thickness) on top of a microporous support (pores 2 nm [16], 40 μm thickness) and a fabric layer (120–150 μm thickness) which supplies mechanical strength [13,17,18]. The PA layer is created on top of the supporting structure through on-surface polymerization of diamine and tricarboxyl monomers. The PA layer is a (highly) cross-linked polymer, and, thus, one of the monomers contains at least three functional groups, two for propagation and one for cross-linking. The membrane can subsequently be coated with another polymer layer (e.g., polyvinyl alcohol, polyethyleneimine), for instance, to supply additional protection from fouling [14,17,19], but this layer can also cause flux reduction [14].

Essential for the PA layer is obviously the presence of pores. In RO, the pores in the membrane refer to the percolated free volume that is present between the polymer chains in the PA layer. The number of pores and the pore size distribution depend on the polymerization process [11]. Compared to nanofiltration membranes, RO membranes have a more narrow size distribution, i.e., a more uniform pore size [20], typically in the range of an average diameter between 0.66 and 0.78 nm [20–22]. Kim and Hoek [23] distinguished two types of pores. The smaller type, "network pores," are defined as the gaps between polymer branches, while "aggregate pores" relate to the spaces between polymer aggregates. Network pores have a smaller size (approximately 0.4–0.5 nm) and constitute about 70% of the pore volume, while aggregate pores (approximately 0.7–0.9 nm) account for the remainder [23,24].

The chemical charge of the PA layer is a consequence of the polymerization process. Carboxylic and amine functional groups that did not participate in the cross-linking process or in chain elongation reactions remain free and can be protonated or deprotonated depending on the *p*H [24]. Protonated amine groups result in positive charge and deprotonated carboxyl groups result in a charge of negative sign. This means that dependent on *p*H the membrane can have a positive or negative charge, as we discuss in more detail in Sec. III E.

TABLE I. Composition of Mediterranean seawater (most common ions only) [26,27].

Species	Concentration (mg/L)
Na^+	12 500
Mg^{2+}	1450
Ca^{2+}	450
K^+	450
Cl^-	22 100
SO_4^{2-}	3410
HCO_3^-	160
B	4–5
*p*H	8.1

B. Seawater characteristics

Seawater is the largest water body available on Earth—a fact that makes it an attractive, inexhaustible source for drinking water. Seawater is characterized by a high salinity ["total dissolved solids" (TDS) > 35 g/L] with sodium and chloride being the major ions. Seawater is slightly basic with a typical *p*H of approximately 8.0. With the development and advances in RO technology over the years, the use of seawater as a source of potable water has increased, at present estimated at 60% of the global intake for RO desalination [25]. Table I presents an example of a typical composition of seawater.

Several acid-base reactions occur in (sea)water, which must be included in the theory. In all cases, we assume that the reaction is infinitely fast, and thus, locally, the ions participating in the reaction are at chemical equilibrium with one another. First of all, we must consider the autoprotolysis reaction of water in which a proton is transferred from one water molecule to an other according to

$$2H_2O \rightleftharpoons H_3O^+ + OH^-, \quad pK_w = 14 \text{ at } 25\,^\circ\text{C}, \text{ pure water}.$$

The value of pK_w for pure water at 25 °C of $pK_w \sim 14$ drops to lower values for more saline solutions [28,29].

Boron is an element present in natural water systems. Seawater contains about 5 mg/L boron [28,30], which is predominantly in one of two forms: boric acid $B(OH)_3$ and the borate ion $B(OH)_4^-$. For boron concentrations higher than 22 mg/L, other species, mainly cyclic forms, may be present as well, depending on *p*H [31]. The distribution between boric acid and borate is given by

$$B(OH)_3 + H_2O \rightleftharpoons H^+ + B(OH)_4^-,$$
$$pK = 9.23 \text{ at } 25\,^\circ\text{C}, \text{ pure water.}$$

It was shown in Ref. [31] that salinity affects pK, bringing it down to $pK = 8.60$ for 40-g/L TDS.

The degree of rejection of boron in seawater RO is of considerable concern. At low concentrations, boron is beneficial for human health such as for cell metabolism, bone density, and the immune system [32,33], but high boron intake can lead to illness [34,35]. The guideline of the World Health Organization is 2.4-mg/L boron [36] (2.0 mg/L according to Ref. [37]). However, this concentration is too high when the water is used in agriculture for irrigation purposes. In this case, a lower boron concentration must be reached, the exact value depending on the crop type [38]. Note that for proper growth of plants, a certain (low) amount of boron is nevertheless required because it participates in cell distribution, growth and metabolism, respiration regulation, and photosynthesis.

In desalination by RO, it is argued that boron in the acid (hydrated) form passes through the RO membrane quite freely while the borate ion is rejected. The borate ion is weakly hydrated and, thus, relatively small [39], and we can assume that boric acid being a neutral species in water will have an even smaller hydrated size [40]. Since boron rejection depends on the distribution between the uncharged and charged form determined by the equilibrium constant, it is expected that pH and temperature influence boron rejection. In addition, the membrane itself can enhance borate ion rejection when it is negatively charged. To facilitate rejection, pH of the feed has to be around 8.0 in order to achieve about 88%–93% rejection [41]. To further reduce boron concentration in the effluent, RO plants must use an additional RO step, boron selective resins, and/or make pH adjustments to meet regulations on boron concentration [42].

Also present in seawater are carbonate ions in several ionic forms. The carbonate system functions as a buffer system in natural water and is the main contributor to the ability of seawater to buffer pH changes. The seawater carbonate system is in equilibrium with CO_2 in air, which dissolves as H_2CO_3 (carbonic acid). For the carbonate system, the equilibria in water are given by

$$CO_2(g) \rightleftharpoons CO_2(aq),$$
$$CO_2(aq) + H_2O \rightleftharpoons H_2CO_3(aq),$$
$$H_2CO_3(aq) \rightleftharpoons H^+ + HCO_3^-,$$
$$pK_{H_2CO_3} = 6.33 \text{ at } 25\,^\circ\text{C}, \text{ pure water},$$
$$HCO_3^- \rightleftharpoons H^+ + CO_3^{2-},$$
$$pK_{HCO_3^-} = 10.33 \text{ at } 25\,^\circ\text{C}, \text{ pure water}.$$

Note that also for the carbonate system, it was shown that pK is a function of salinity, resulting in $pK_{H_2CO_3} = 5.98$ and $pK_{HCO_3^-} = 9.16$ for a 30-g/L salt solution at 25 °C [43,44]. In RO, it is known that the permeate only contains very low levels of HCO_3^- and CO_3^{2-}. The rejection of carbonate by RO membranes, therefore, increases carbonate concentrations in the retentate (brine), which can lead to "scaling," which is the precipitation of components such as $CaCO_3$ and $MgCO_3$ on the membrane surface.

In our work, the above equilibria are combined with the relevant transport equations which are set up for each ion individually. The resulting coupled model has an inherent complexity, which lies in the fact that in addition to transport, species can form and react away due to the various chemical equilibria.

C. Concentration polarization

Every membrane separation process promotes the passage of some species over others. This selective permeation leads to gradients in concentration in the boundary layer in front of the membrane. For RO, if the species is rejected by the membrane, it will accumulate on the surface, resulting in a higher concentration [Fig. 1(a)], and if the membrane favors its passage, the ion will deplete [Fig. 1(b)]. In RO, typically the salt concentration on the membrane surface is increased, creating concentration gradients in a boundary layer between bulk solution and membrane surface. This phenomenon of concentration polarization (CP) is of importance in RO systems because it leads to a larger salt concentration difference across the membrane and an increase in osmotic pressure of the solution on the surface of the membrane. In addition, it promotes scaling and "cake-layer" development on the membrane surface. These combined effects eventually result in a reduction of performance of the RO system.

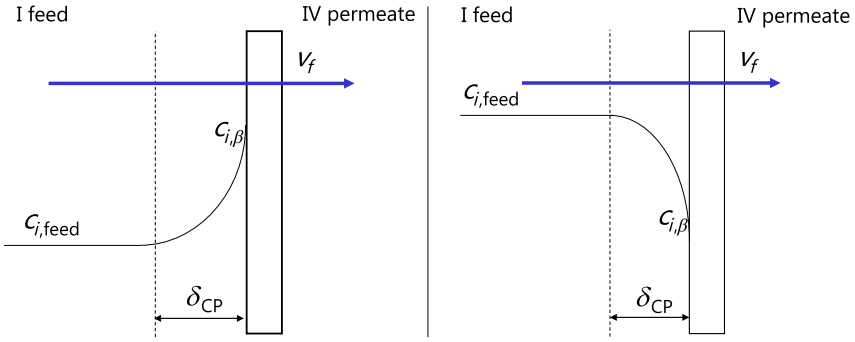

FIG. 1. Sketch of concentration polarization in reverse osmosis for the case when (a) a component is enriched at the membrane surface and (b) when a component is depleted. Situation (a) is the typical situation in RO when ionic species are rejected by the membrane, but for some species, the opposite behavior is possible.

III. MODEL EQUATIONS

To model ion rejection and water recovery by RO membranes, appropriate transport models must be set up. Traditionally, two important mechanistic models have been used which are the solution-diffusion (SD) model and the fine capillary pore (FCP) model [45]. In the SD model, the three transport steps of adsorption, diffusion, and desorption are each considered. The case of separating water from dissolved salts results in simplified transport equations due to additional assumptions such as a constant water (solvent) concentration in the membrane and an equal total pressure on the boundary between the membrane and feed side. The SD model provides two membrane parameters which can be determined experimentally, and, thus, the SD approach offers a method to estimate and plan an RO process. Yet this model simplifies the actual transport mechanisms extensively and does not describe the complexity of the system and acting forces in detail. Instead, the FCP model describes the film layer as a porous layer with pores of a certain size through which the hydrated ions move. The support layer can also be included in this way, only with much larger pores, but it is usually neglected in the theory.

A general description of our modeling framework is presented in Fig. 2. Like in the FCP model, in the present work we describe the active layer (III) as a porous material with tortuous pores of a uniform size. This size is only somewhat larger than that of the ions and thus hinders their movement. We describe transport using a Maxwell-Stefan approach, considering three contributions to ion transport: concentration gradients (diffusion), potential gradients (electromigration), and advection of ions with the flow of water. For uncharged species, such as boric acid and carbonic acid, there is no migration term involved, and their transport is governed by diffusion and advection only. We neglect the friction between ions, but for all ions, we include their friction with the fluid (the "free" water) as well as with the membrane. Steric partitioning and the Donnan effect are included at both membrane-solution interfaces (β,γ). The phenomenon of concentration polarization in a layer in front of the membrane is included on the membrane-feed side (II).

A. Molecular flux of ions

We aim to describe the simultaneous flow of the components in the water matrix through a realistic membrane with a certain porosity and tortuosity of the pores. The derivation starts with a description of a single pore, one which not necessarily follows the shortest distance across the membrane (the "direct direction") but instead follows a tortuous path (with a coordinate along the pore x') that is longer by a factor of τ. Inside such a pore, Maxwell-Stefan theory results in a relationship between the driving forces acting on an ion and the frictions that it encounters given by

$$-\nabla\mu_i = R_g T \sum_j \zeta_{i-j}(v'_i - v'_j), \tag{1}$$

where μ_i is the electrochemical potential of the ion, ζ_{i-j} is a factor describing the friction between species i and j, R_g is the gas constant, T is temperature, and v'_i and v'_j are the velocities of the ions in the pore, following the path of the pore. We neglect the friction between different ionic species and consider only the friction of ions with the membrane (m) and with the free water in between the hydrated ions (which has velocity v'_f, where subscript "f" is for fluid). In that case, Eq. (1) can be written in the x' direction as

$$-\frac{1}{R_g T}\frac{\partial \mu_i}{\partial x'} = \zeta_{i-m}(v'_i - v'_m) + \zeta_{i-f}(v'_i - v'_f), \tag{2}$$

where since the membrane is static, we have $v'_m = 0$. We assume ideal thermodynamic behavior for the ions (i.e., we neglect the volumetric interactions discussed in Ref. [46]), and, thus, the electrochemical potential μ_i is given by

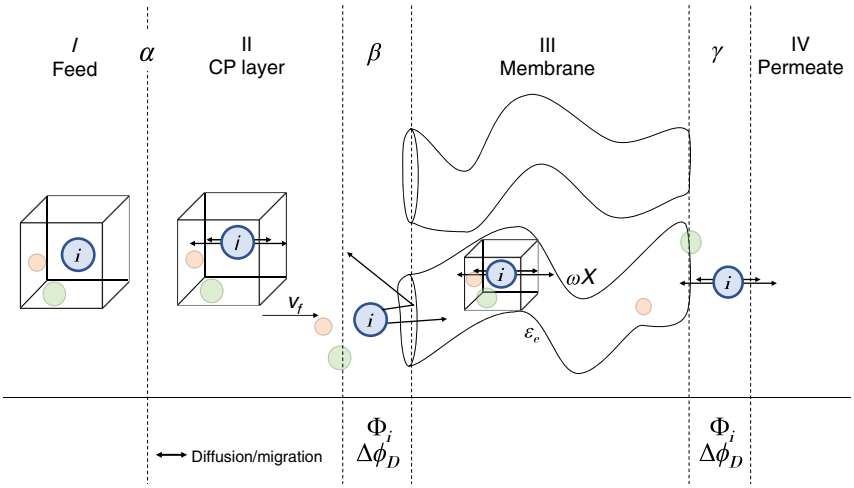

FIG. 2. Description of the reverse-osmosis model used in this work. α, β, and γ represent the three boundaries in the system: feed-CP layer, CP-layer membrane, and membrane permeate.

$$\mu_i = \mu_{i,0} + R_g T(\ln c_i + z_i \phi), \tag{3}$$

where c_i and z_i are the concentration and valency of species i, and ϕ is the dimensionless electric potential. We can insert Eq. (3) in Eq. (2) which results after rearrangement in

$$v_i' = \left(\frac{\zeta_{i-f}}{\zeta_{i-f}+\zeta_{i-m}}\right) v_f' - \frac{1}{\zeta_{i-f}+\zeta_{i-m}}\left(\frac{\partial \ln c_i}{\partial x'} + z_i \frac{\partial \phi}{\partial x'}\right). \tag{4}$$

Equation (4) shows a striking similarity to expressions from hydrodynamic theory for hindered transport of spherical particles in cylindrical pores [47,48],

$$v_i' = K_{c,i} v_f' - K_{d,i} D_{\infty,i}\left(\frac{\partial \ln c_i}{\partial x'} + z_i \frac{\partial \phi}{\partial x'}\right), \tag{5}$$

where $K_{c,i}$ and $K_{d,i}$ are called hindrance factors for convection and diffusion. These factors are only a function of the ratio between the diameter of the ion and the pore [47,49]. Comparing Eqs. (4) and (5) shows that $K_{c,i} = \zeta_{i-f} K_{d,i} D_{\infty,i}$.

Up to this point, transport is considered within a single pore, along a pore coordinate x'. However, we need to develop a model for fluxes in an actual membrane where part of the structure is not accessible to ions and water and where the paths of the pores are tortuous and longer than the shortest direction across the membrane. To account for this, we first implement $dx' = \tau dx$, with τ tortuosity, where x is the coordinate following the shortest distance across the membrane (which we call the "direct direction"). This modification corrects for the fact that in a real pore, the average driving force is lower than what it would have been when oriented straight across the membrane. Velocities v' used above, which are defined along x', the direction of the tortuous pore, relate to a superficial velocity v (per unit total membrane area, in the direct direction) by $v = v'\epsilon/\tau$ where ϵ is the membrane porosity. Inserting these relations between x' and x and between v' and v in Eq. (5) leads to

$$v_i = K_{c,i} v_f - K_{d,i} \varepsilon_e D_{\infty,i}\left(\frac{\partial \ln c_i}{\partial x} + z_i \frac{\partial \phi}{\partial x}\right), \tag{6}$$

where $\varepsilon_e = \epsilon/\tau^2$, and multiplying Eq. (6) with c_i results in (for the flux of ion type i)

$$J_i = K_{c,i} c_i v_f - K_{d,i} \varepsilon_e D_{\infty,i}\left(\frac{\partial c_i}{\partial x} + z_i c_i \frac{\partial \phi}{\partial x}\right). \tag{7}$$

B. Water flow

Also, for the water (fluid) in the pore, we must set up a Maxwell-Stefan-based expression relating the fluid velocity v_f to the velocities of ions and driving forces acting on the water. For the water, the required expression is closely related to Eq. (1), which in the above section is used to describe the flux of ions. Equation (1) is a force balance on one ion (1 mole of ions), which has friction with the water (filling all space between the ions), pore walls, and other ions. For water, we set up a balance per pore volume V; thus, the left-hand side of Eq. (1) becomes $-\nabla\mu_w c_w(1-\eta)V$, where c_w is the concentration of water (in water), which is given by $c_w = 1/V_w$, where V_w is the molar volume of a water molecule, and where η is the volume fraction of all (hydrated) ions in the pore (i.e., the volume excluded for free water), which we set to zero from this point onward.

For the friction exerted on the water that is in a volume V, we start with the expression on the right-hand side of Eq. (1), multiplied again by V and for the water-ion frictions multiplied by the concentration of ions, not of the water. This difference can be understood from the fact that the right-hand side of Eq. (1) describes the friction of one ion (or 1 mole of ions) with the continuum phase of water (and pore walls, and other ions), but we are now interested in the friction of all water that is in a volume V with all ions present in that volume. Next, we implement in the resulting equation, that the chemical potential for the water molecules is given by

$$\nabla\mu_w = V_w R_g T \nabla P^t, \tag{8}$$

where the total pressure P^t is given by [50]

$$P^t = P^h - \Pi, \tag{9}$$

where P^h and Π are the hydraulic and osmotic pressure, both in units of mol/m^3 (meaning, pressure in pascals divided by $R_g T$). For ideal molecules, i.e., without volume effects, the osmotic pressure is a summation of species concentrations (excluding water molecules), $\Pi = \sum_i c_i$ [50–52]. Finally, we include a term for friction between the water and pore walls and then arrive at [51]

$$\frac{\partial P^t}{\partial x'} = -f'_{f-m} v_f' + \sum_i \zeta_{i-f} c_i (v_i' - v_f'), \tag{10}$$

where the first term on the right-hand side relates to the friction of water (fluid) with the pore walls (which have zero velocity), and the summation in the second term runs over all ions (not water).

In the above derivations for transport of ions and free water in the pore, an assumption is that the ions occupy no volume when we equate velocity v_f' in Eq. (2) with that in Eq. (5) and when we neglect the effect of ion volume in Eq. (3) and in the derivation of Eq. (10). Note, however, that in the calculation of partition coefficients

and hydrodynamic hindrance functions, ion volume does play a role.

Inserting Eq. (6) in Eq. (10) and making the conversions from x' to x and v' to v results in

$$-\frac{\partial P^t}{\partial x} = \frac{1}{\varepsilon_e}\left(f'_{f-m} + \sum_i c_i \zeta_{i-f}(1 - K_{c,i})\right) v_f + K_{c,i}\left(\frac{\partial}{\partial x}\sum_i c_i - \omega X \frac{\partial \phi}{\partial x}\right), \tag{11}$$

where we implemented the local electroneutrality condition in the membrane

$$\sum_i z_i c_i + \omega X = 0, \tag{12}$$

where ωX is the membrane charge density to be discussed in detail in the next section. By setting $K_{c,i} = 1$ (i.e., no ion-wall friction), Eq. (11) results in the classical expression [53]

$$\frac{\partial P^h}{\partial x} + f_{f-m} v_f = \omega X \frac{\partial \phi}{\partial x}, \tag{13}$$

where $f_{f-m} = f'_{f-m}/\varepsilon_e$. In the model, Eq. (11) is used to describe the change in P^t across the membrane, while at the membrane edges, P^t is continuous (i.e., it does not change).

In the following sections, we describe further elements of the model relating to pore and ion sizes, partitioning at membrane edges, hindrance factors, and membrane charge.

C. Effective ion and pore sizes in PA membrane

In our model, we assume that the main resistance to transport in the membrane derives from the PA layer, and, therefore, the membrane description is of that layer alone. The layer is considered to be a rigid structure [11,20,54], and, thus, we choose a defined (average) pore size. We use for the pore size a value of 0.76 nm [20,55] and for the film thickness $\delta_m = 100$ nm. These values are within the range of numbers reported in the literature [11,18,20,22,24,55,56]. Owing to the aqueous environment in the membrane, the species are described with their solvation shell included. However, since the hydrated size of the carbonate and bicarbonate ions exceeds the chosen value for pore size, we must assume that they have to at least partially shed their hydration shell to fit in the pore. The reduced sizes for these two ions are still significantly larger than for the neutral carbon acid [40]. All ion sizes used in the model are summarized in Table II.

D. Donnan-steric partitioning

As a result of the membrane charge, an electrochemical potential develops on both membrane edges (denoted as β and γ in Fig. 2). This phenomenon is known as the Gibbs-Donnan effect, and the electric potential difference is known as the Donnan potential. Based on the calculated value of the Donnan potential, we can relate the concentration of the ions on both sides of the boundary. In addition, we also account for a steric hindrance of the ion in the pore by introducing a partitioning coefficient at the membrane-solution interface described by

$$\Phi_i = (1 - \lambda_i)^2, \tag{14}$$

where λ is the ratio between ion size and pore size. Combining partitioning and electrostatic effects, we obtain

$$c_{i,m} = c_{i,\infty} \Phi_i \exp(-z_i \Delta\phi_D), \tag{15}$$

where $\Delta\phi_D$ is the dimensionless Donnan potential (Donnan potential divided by $R_g T/F$), and subscript m refers to a point just within the membrane and ∞ to just on the outside. It has been suggested that for the ions to enter the pores, they must (partially) dehydrate, which leads to an energy barrier [24,63]. This energy can easily be included in the Donnan balance, leading to an extra constant factor that we can combine with the term Φ_i above. Thus, when an ion size is chosen empirically, smaller than the fully hydrated size (as we do for the carbonate ions), then this automatically includes a desolvation energy.

E. Membrane charge

Coronell *et al.* quantified the charged functional groups in a FT30 RO membrane [24]. They found that while ionized amine groups can be described by one dissociation constant pK_{NH_2}, two values were required for the carboxylic groups, which we denote by pK_{COOH_1}, pK_{COOH_2}. The equilibrium constant K_{COOH} of the deprotonation of the carboxylic acid $[RCOOH] \rightleftharpoons [H^+] + [RCOO^-]$ (where R represents the polymer backbone) is given by

$$K_{COOH} = \frac{[H^+][RCOO^-]}{[RCOOH]}, \tag{16}$$

and due to the fixed number of carboxylic groups $X_{COOH} = [RCOO^-] + [RCOOH]$, we arrive at

$$[RCOO^-] = X_{COOH} \Big/ \left(1 + \frac{[H^+]}{K_{COOH}}\right). \tag{17}$$

Similarly, for the amine groups, the equilibrium $[RNH_3^+] \rightleftharpoons [H^+] + [RNH_2]$ leads to

TABLE II. Input values used in all calculations.

	Parameter	Value	Parameter	Value
Constituents	Na^+_{feed}	553 mM	pK_{COOH_1}	5.23 [24]
	Cl^-_{feed}	550 mM	pK_{COOH_2}	8.97 [24]
	$Btot_{feed}$	0.5 mM [27,57]	pK_{NH_3}	4.74 [24]
	$Ctot_{feed}$	2.48 mM [26,58]	$pK_{B(OH)_3}$	8.60 [44]
	pH_{feed}	8.0 [26,27]	$pK_{H_2CO_3}$	5.98 [28]
			$pK_{HCO_3^-}$	9.16 [28]
			pK_w	13.3 [28]
Properties	d_{Na^+}	7.16 Å [59]	d_{Cl^-}	6.64 Å [59]
	$d_{H_3O^+}$	5.64 Å [59]	d_{OH^-}	6.00 Å [59]
	$d_{B(OH)_3}$	3.84 Å[a]	$d_{B(OH)_4^-}$	5.22 Å [39]
	$d_{H_2CO_3}$	3.64 Å[a]	$d_{HCO_3^-}$	7.16 Å[b]
	$d_{CO_3^{2-}}$	7.30 Å[b]	d_{pore}	7.60 Å [20,55]
	$D_{H_3O^+}$	8.24×10^{-9} m^2/s [19]	D_{OH^-}	4.51×10^{-9} m^2/s [19]
	D_{Na^+}	1.33×10^{-9} m^2/s [60]	D_{Cl^-}	2.00×10^{-9} m^2/s [60]
	$D_{B(OH)_3}$	1.28×10^{-9} m^2/s [61]	$D_{B(OH)_4^-}$	1.18×10^{-9} m^2/s
	$D_{H_2CO_3}$	1.92×10^{-9} m^2/s [62]	$D_{HCO_3^-}$	1.18×10^{-9} m^2/s [62]
	$D_{CO_3^{2-}}$	9.8×10^{-10} m^2/s [62]		
Membrane	δ_m	100 nm [18,24,55]	δ_{CP}	20 μm [3]
	ε_e	0.05 [55]	f_{f-m}	1.3×10^{14} mol s/m^5[c]
	X_{COOH_1}	82 mM [24]	X_{COOH_2}	350 mM [24]
	X_{NH_3}	36 mM [24]		
Partitioning (calculated)	λ_{Na^+}	0.942	λ_{Cl^-}	0.874
	$\lambda_{H_3O^+}$	0.742	λ_{OH^-}	0.790
	$\lambda_{B(OH)_3}$	0.505	$\lambda_{B(OH)_4^-}$	0.687
	$\lambda_{H_2CO_3}$	0.479	$\lambda_{HCO_3^-}$	0.942
	$\lambda_{CO_3^{2-}}$	0.961		
	Φ_{Na^+}	0.003 35	Φ_{Cl^-}	0.0156
	$\Phi_{H_3O^+}$	0.0665	Φ_{OH^-}	0.0443
	$\Phi_{B(OH)_3}$	0.245	$\Phi_{B(OH)_4^-}$	0.0981
	$\Phi_{H_2CO_3}$	0.272	$\Phi_{HCO_3^-}$	0.003 35
	$\Phi_{CO_3^{2-}}$	0.001 56		
Hindrance (calculated)	K_{c,Na^+}	0.287	K_{d,Na^+}	0.005 54
	K_{c,Cl^-}	0.519	K_{d,Cl^-}	0.0102
	K_{c,H_3O^+}	0.676	K_{d,H_3O^+}	0.0202
	K_{c,OH^-}	0.644	K_{d,OH^-}	0.0137
	$K_{c,B(OH)_3}$	0.832	$K_{d,B(OH)_3}$	0.161
	$K_{c,B(OH)_4^-}$	0.714	$K_{d,B(OH)_4^-}$	0.0373
	K_{c,H_2CO_3}	0.848	K_{d,H_2CO_3}	0.188
	K_{c,HCO_3^-}	0.287	K_{d,HCO_3^-}	0.005 54
	$K_{c,CO_3^{2-}}$	0.205	$K_{d,CO_3^{2-}}$	0.003 93
	R_g	8.3144 J/K/mol	T	25 °C
	F	96 485 C/mol		

[a]Based on Stokes-Einstein relation using $\mu_w = 8.9 \times 10^{-4}$ Pa s [61].
[b]Partial loss of hydration shell is assumed.
[c]Based on $f_{f-m} = (A\delta_m R_g T)^{-1}$ [51], with $A = 3.0\,\mu$m/bar/s [18].

$$[RNH_3^+] = X_{NH_2} \Big/ \left(1 + \frac{K_{NH_2}}{[H^+]}\right). \tag{18}$$

Thus, for the membrane charge ωX at any position in the PA layer (as a function of local pH), we arrive at

$$\omega X = X_{NH_2} \Big/ \left(1 + \frac{K_{NH_2}}{[H^+]}\right) - X_{COOH_1} \Big/ \left(1 + \frac{[H^+]}{K_{COOH_1}}\right) - X_{COOH_2} \Big/ \left(1 + \frac{[H^+]}{K_{COOH_2}}\right), \tag{19}$$

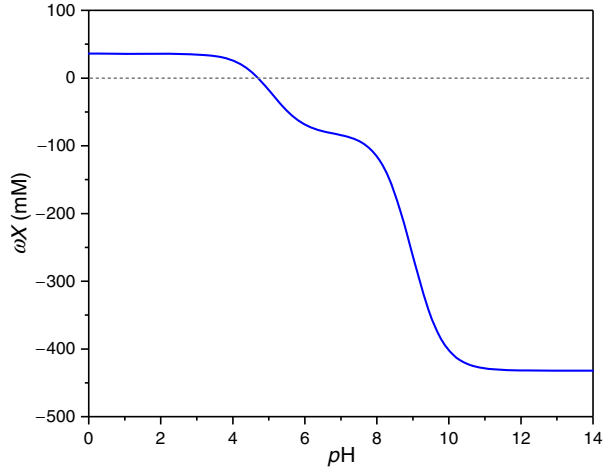

FIG. 3. Membrane charge in the RO polyamide layer as function of pH, based on Ref. [24].

which is also applicable in our model when these acid-base reactions are relatively slow, because we assume steady-state operation of the process. The result of Eq. (19) is plotted as a function of pH in Fig. 3 based on the data in Ref. [24]. Though the membrane charge as measured in Ref. [24] is a concentration per unit total volume of the PA layer, we will use their result as if it is the membrane charge per unit pore volume.

F. Hindered transport

Since the pore size is not much larger than the ion sizes, it is important to include both sizes in the transport model. Here, we rely on hydrodynamic theory for hindered transport [47,49], which results in expressions for the steric hindrance coefficients. These expressions depend on the size ratio: for $0 < \lambda_i < 0.8$, the expression is adapted from Bowen *et al.* [64], and for $0.8 < \lambda_i < 1$, it is based on Bandini and Vezzani [65]. They are given by

$$K_{c,i} = \begin{cases} 1.0 + 0.054\lambda_i - 0.988\lambda_i^2 + 0.441\lambda_i^3, & 0 < \lambda_i < 0.8, \\ -6.83 + 19.348\lambda_i - 12.518\lambda_i^2, & 0.8 < \lambda_i < 1, \end{cases}$$
$$K_{d,i} = \begin{cases} 1.0 - 2.30\lambda_i + 1.154\lambda_i^2 + 0.224\lambda_i^3, & 0 < \lambda_i < 0.8, \\ -0.105 + 0.318\lambda_i - 0.213\lambda_i^2, & 0.8 < \lambda_i < 1. \end{cases} \tag{20}$$

For each of the ions, the input values for λ_i and the calculated values for $K_{c,i}$ and $K_{d,i}$ are presented in Table II.

G. Concentration-polarization layer

For the description of the CP layer in front of the membrane, the same transport equations are used as presented above for the PA layer but now excluding hindered transport and the porosity and tortuosity effects. Thus, in the CP layer, the ionic flux is described by the Nernst-Planck equation

$$J_i = c_i v_f - D_{\infty,i}\left(\frac{\partial c_i}{\partial x} + z_i c_i \frac{\partial \phi}{\partial x}\right), \tag{21}$$

while Eq. (13) results in the fact that in the CP layer the hydrostatic pressure gradient is zero. Electroneutrality in the CP layer is described by Eq. (12) with $\omega X = 0$.

H. Auxiliary relations for ionic fluxes

Several additional relations are required to obtain a complete model. First of all, in RO, the ionic current $J_{\rm ch}$ is zero, and, thus, the summation of all ion fluxes (times valency) must be zero at each point in the CP layer, as well as at each point in the membrane. Thus, at each point we have

$$J_{\rm ch} = \sum_i z_i J_i = 0. \tag{22}$$

Until now, we have not yet explicitly described how the acid or base reactions play a role in the structure of the model. As we mentioned in Sec. II B, transport of weak acid systems, such as boric acid and carbonic acid, is more complicated to describe than transport of "inert" ions because of the local chemical equilibria that are affecting concentrations. In our model, we take into consideration that all species, except for sodium and chloride, relate to other ions through one or more chemical equilibria. This means that a change in the concentration of one ion, for instance, HCO_3^-, will actuate a change in concentration of other ions, such as H_2CO_3, HCO_3^-, H_3O^+, and OH^-, and also indirectly have an influence on the concentration of yet other ions, $B(OH)_3$ and $B(OH)_4^-$ in our case. As a consequence of these equilibria, it is not the flux of an individual ion, like HCO_3^-, that is invariant across the membrane but only the flux of certain *groups* of ions, such as the group formed of the three carbonate species [62]. The same holds for the group of the two boron species. Note that it is not necessary to set up an ion mass balance in H_3O^+ and OH^- [62], but these species enter the code via the chemical equilibria and via the zero-current condition of Eq. (22).

Finally, we need to relate the concentration in the permeate to the fluxes through the membrane. When on the permeate side there is no fluid flow along the membrane, we have

$$c_{i,\rm permeate} = J_i / v_f. \tag{23}$$

It is important to note that in this form, Eq. (23) can be used only for Na^+ and Cl^-. For the carbonate and borate groups, Eq. (23) is used for the flux and concentration of the entire group. Equation (23) should not be used for H_3O^+ and OH^-.

All flux equations are discretized and solved in the steady state by methods similar to those in Ref. [62] for a

given feed composition and fluid flow rate v_f. The hydrostatic pressure difference ΔP^h required to achieve a given flow rate is calculated afterward. Rejection by the membrane of an ion or group of ions is defined as $R_i = 1 - c_{i,\text{permeate}}/c_{i,\text{feed}}$. This definition is used for Na^+, for the group of the three carbonate species, and for the group of the two boron species. For Na^+ and for Cl^-, the rejection is almost the same, and in the next section, it is denoted as R_{NaCl}.

IV. RESULTS AND DISCUSSION

A. Input parameters in the model

In this section, we present calculation results for one seawater composition and one set of input parameters for ion size, diffusion coefficients, etc. The only parameters that are changed are the water flow rate through the membrane v_f, membrane charge, and seawater feed pH. All input parameters used in the model are listed in Table II. Note that from here on, the word membrane refers to the PA top layer in a commercial RO membrane, while "(free) water" and "fluid" both refer to the water molecules that fill the space around the solvated ions.

B. Results as a function of the permeate flow rate

Before investigating the influence of water flow rate, we first present calculation results for a permeate flow rate (water flow rate through the membrane) of $v_f = 10$ μm/s, which is a typical value in seawater reverse osmosis, and which recalculates to 36 L/m^2/h [3]. The performance of the membrane at this condition in terms of rejection of salt and boron is summarized in Table III and compared with values from literature. As shown in Table III, we obtain a very good match for all three properties. The model gives a somewhat too optimistic prediction of salt and boron rejection, which can be resolved by using a slightly larger pore size in the calculation (for a pore size of 0.78 nm, $R_{\text{NaCl}} = 99.7\%$, $R_{\text{B}} = 91.1\%$, and $p\text{H}_{\text{permeate}} = 8.51$). The calculated $p\text{H}_{\text{permeate}}$ is within the range of data reported in Ref. [66]. An elevation in $p\text{H}_{\text{permeate}}$ compared with $p\text{H}_{\text{feed}}$ was also observed in Ref. [67] with a feed (seawater) pH of 9.0 resulting in a permeate pH of 9.1–9.5. According to Eq. (11), for this water flow rate, the required applied pressure is $\Delta P^h = 35.6$ bar. Based on this value and the osmotic

TABLE III. Summary of model output compared with experimental values for seawater reverse osmosis reported in the literature.

Parameter	Our model	Literature	Reference
$p\text{H}_{\text{permeate}}$	8.75	8.6–8.8	[66]
R_{NaCl}	99.9%	96.6%–99.8%	[69]
R_{B}	93.5%	87%–93%	[69]

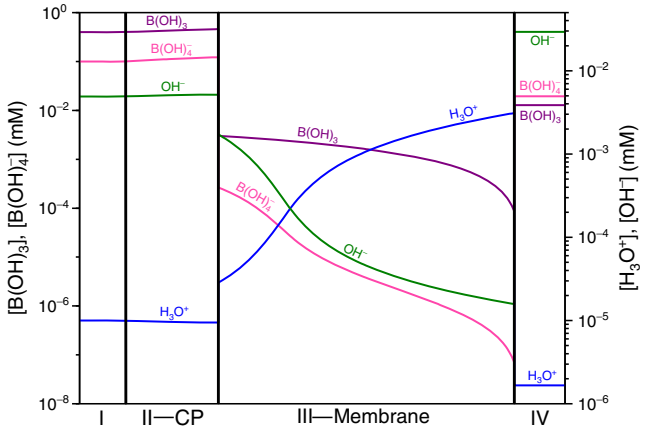

FIG. 4. Concentration profiles of the two boron species and H_3O^+ and OH^- in the CP layer (II) and membrane (III). Concentrations are plotted on a logarithmic scale. Left is the feed solution (I), right is the permeate (IV).

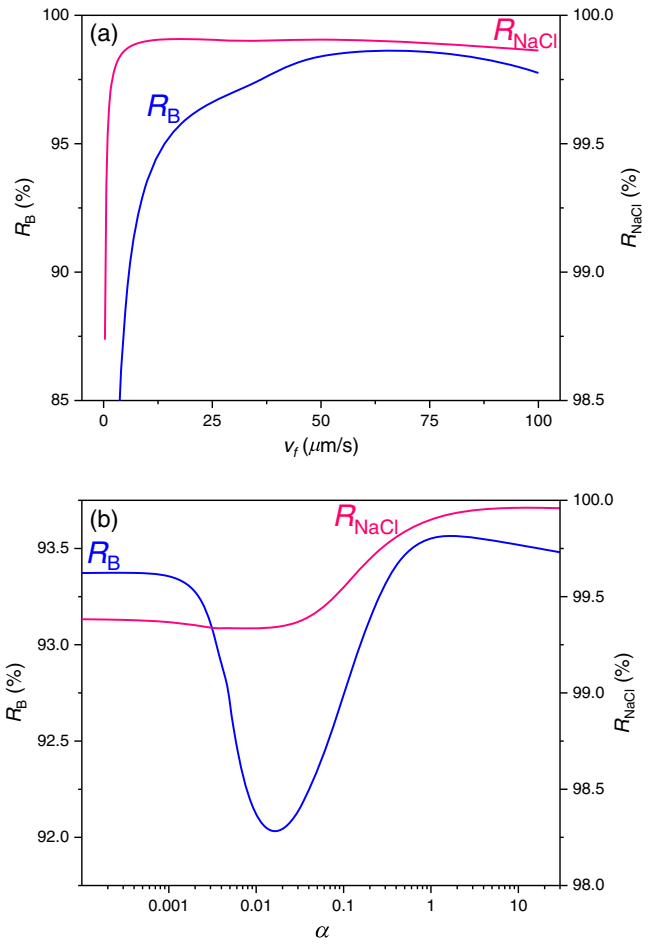

FIG. 5. Rejection of NaCl and boron by the membrane as function of (a) water flow rate v_f and (b) membrane charge density α, which is the factor by which the concentration of each component of membrane charge X_k is multiplied. Conditions of Table II, $v_f = 10$ μm/s.

pressure of the feed solution, the thermodynamic efficiency of this process can be calculated as $\eta = 77\%$ based on $\eta = \Delta\Pi/\Delta P^h$ where the osmotic pressure difference is that across the membrane. Note that this relation is valid only for a very low water recovery and a very dilute permeate, see Eq. (3) in Ref. [68].

The calculation shows that the CP layer increases the salt concentration from $c_{\text{salt,feed}} = 550$ mM in the feed to about $c_{\text{salt},\beta} = 620$ mM on the membrane surface. This is roughly a 10% increase, which is less than a typical value reported for RO of around 30% [3]. Thus, in our calculation, the CP layer increases the osmotic pressure of the salt solution directly near the membrane surface by only approximately 4 bar. As observed in the calculations at different values of v_f, for all species but H_3O^+, increasing v_f always results in an increase in ion concentration at the membrane surface.

As an example, we show in Fig. 4 the concentration profiles in the CP layer and in the membrane for the boric acid and the borate ion, as well as for H_3O^+ and OH^-. For H_3O^+ and OH^-, the product of their concentrations is always the same, and, therefore, their profiles are mirror images. Acid or base neutrality pH 6.65 (because $pK_w = 13.3$) is reached at a point around one-third into the membrane. The pH decreases by about 2 points when we move from the very left to the very right of the membrane, while pH increases by 3 points when we exit the membrane. In the membrane, the neutral boric acid molecule is about an order of magnitude more prevalent than the borate anion.

Next, we examine the effect of the fluid flow rate (through the membrane) on system performance both for much lower and much higher flow rates than the standard situation just discussed. Salt rejection remains almost constant throughout the examined range at a value between 99.0% and 99.9% [see Fig. 5(a)], while boron rejection increases from 93.5% at $v_f = 10$ μm/s to $R_B = 98.6\%$ at $v_f = 60$ μm/s. Lower flow rates reduce boron rejection

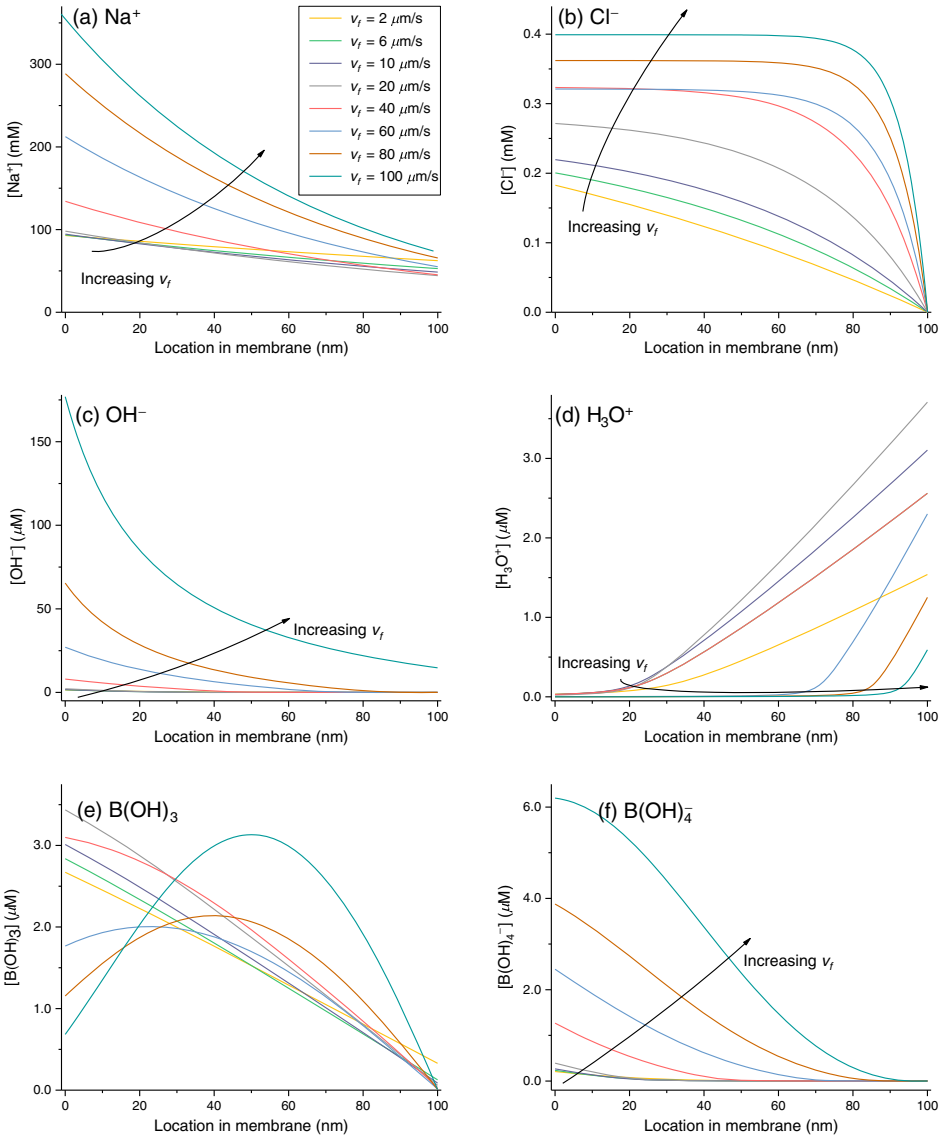

FIG. 6. Concentration profiles in the membrane of Na^+, Cl^-, H_3O^+, OH^-, $B(OH)_3$, and $B(OH)_4^-$ for different values of the water flow rate v_f.

significantly. Increasing the flow rate from 10 to 40 μm/s, the permeate pH decreases from 8.8 to approximately 8.6, after which it increases again to reach a pH of 9.5 at a flow rate of 100 μm/s (results not shown). Thus, for all flow rates, $p\mathrm{H}_{\mathrm{permeate}}$ is higher than the feed pH.

Figure 6 shows concentration profiles of the different ionic species in the membrane for different water flow rates v_f. Such a representation of calculation output is not found in the surveyed literature and highlights the complex characteristic of multicomponent transport in membrane processes. In general, it can be seen that when v_f increases, so does the ion concentration at the feed side of the membrane (left in Fig. 6), except for the hydronium ion.

When we look at two neutral compounds, boric acid (Fig. 6) and carbonic acid (Fig. 7), we see that as v_f increases, so does the concentration at the feed side of the membrane until the trend reverses for $v_f > 20$ μm/s. With higher v_f, the concentration profile for boric acid becomes paraboliclike. For carbonic acid and bicarbonate, their concentration profiles become nonmonotonic, and at some position the concentration is at a maximum. This position shifts away from the feed side when the water flow rate increases.

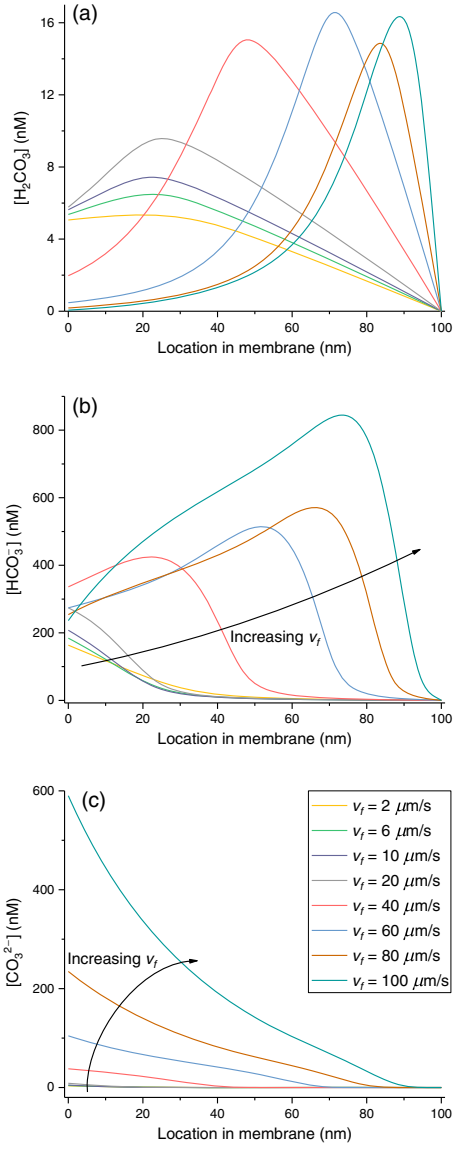

FIG. 7. Concentration profiles in the membrane of H_2CO_3, HCO_3^-, and CO_3^{2-} for different values of the water flow rate v_f.

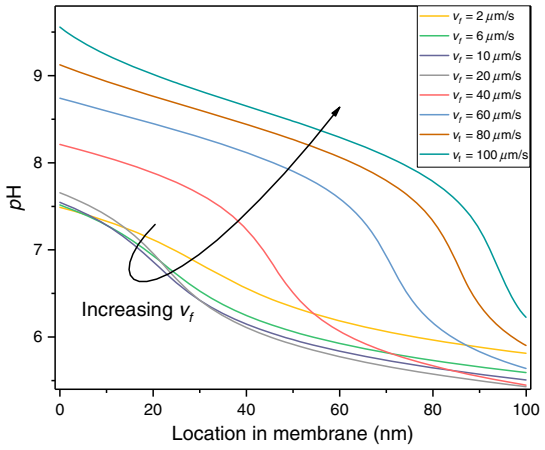

FIG. 8. H_3O^+ concentration in the membrane expressed as pH, for different values of the water flow rate v_f.

pH profiles in the membrane are shown in Fig. 8. At low water flow rates ($v_f \lesssim 36$ μm/s), pH on the feed side of the membrane is lower than $p\mathrm{H}_{\mathrm{feed}} = 8$, while for higher water flow rates, the solution is more basic here. On the permeate side, pH always remains more acidic than in the feed. At the same time, $p\mathrm{H}_{\mathrm{permeate}}$ is always higher than in the feed.

C. Sensitivity analysis

An interesting question is, what is the relative contribution of the three mechanisms that transport ions through the membrane (diffusion, migration, and advection). To analyze that question, the *magnitudes of* the three terms in Eq. (6) are separately calculated and compared. The results in Fig. 9 are based on the standard condition described in Table II with water flow rate $v_f = 10$ μm/s. We present here only the diagrams for selected species. For the other species, the behavior is as follows. For Na^+, the contribution of each mechanism is invariant across the membrane with 23% diffusion, 50% migration, and 27% advection. For OH^-, diffusion and migration are approximately the same as for H_3O^+, and advection is slightly higher. The profiles for HCO_3^- and CO_3^{2-} are similar to $B(OH)_4^-$. For $B(OH)_3$, there is no migration, and diffusion linearly increases from 90% at the feed side to 100% at the permeate side of the membrane.

As Fig. 9 shows, transport of all species that are present at low concentration is dominated by diffusion. This

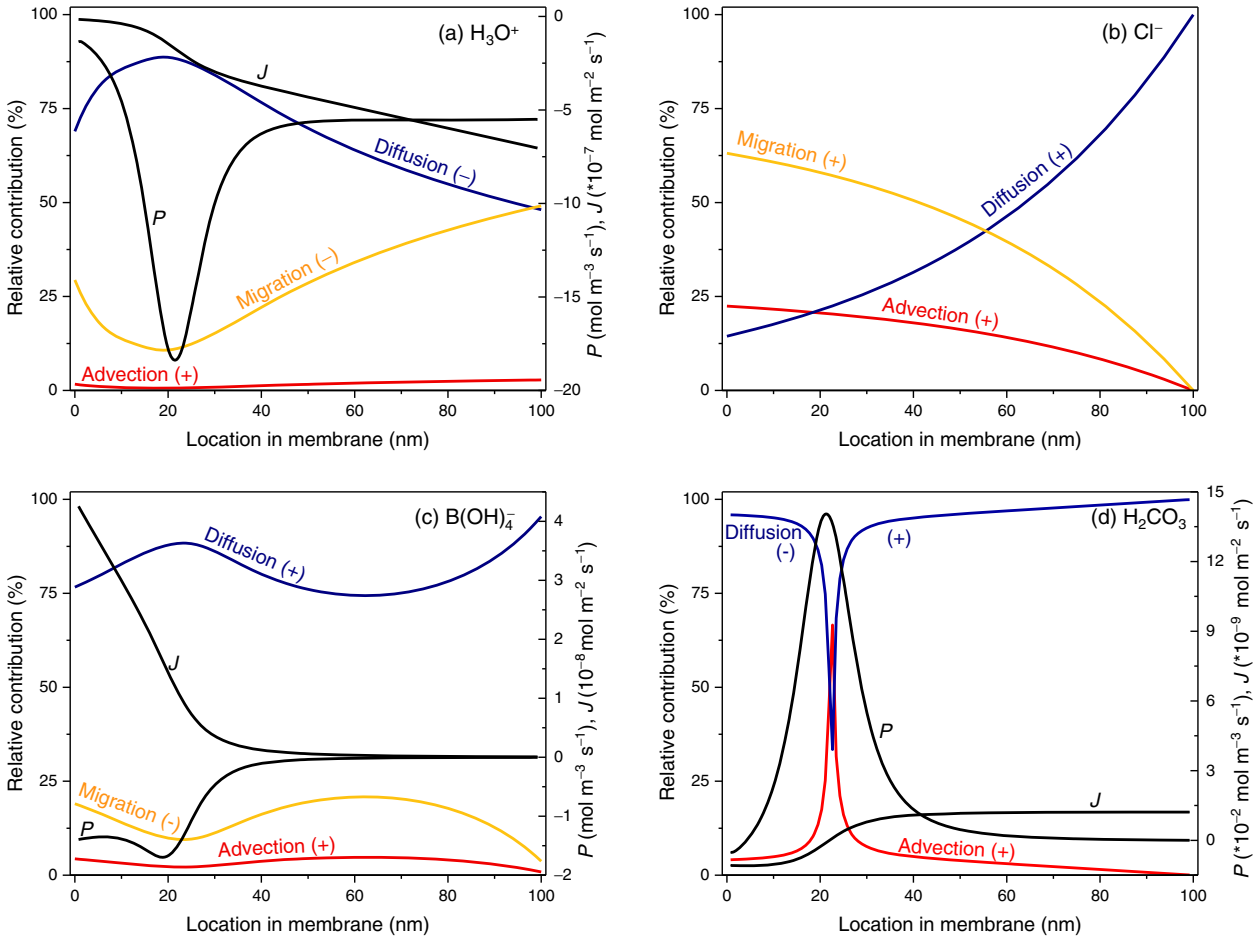

FIG. 9. Relative contribution of diffusion, migration, and advection to the flux of selected ions H_3O^+, Cl^-, $B(OH)_4^-$, and H_2CO_3. Signs next to each line describe whether the term works to move the ion toward the permeate (+) or toward the feed side (−). Also shown is ionic flux J and production rate P.

contribution of diffusion was also discussed for H_3O^+ and OH^- in Ref. [9]. Other than that, the relative contribution of each term is not directly intuitive, for instance, for Cl^- changing strongly across the membrane, while for carbonic acid, an extremely sharp change is observed at some point, due to the fact that at that point the diffusional contribution is zero, and only advection plays a role. Clearly, the study of the relative importance of the various mechanisms driving an ion is nontrivial and may lead to interesting insights. Furthermore, three of the four ions discussed in Fig. 9 are part of an acid or base equilibrium, and, thus, they can react away or be formed within the membrane. This implies that their flux J changes with position because of the production of ions P, as shown in Fig. 9. Because we consider the steady state, the production term P is equal to the gradient in J.

D. Effect of membrane charge

Finally, we investigate the effect of the chemical charge of the membrane. To that end, the standard values of the three functional groups' concentrations X_k are multiplied by a certain factor α, thus keeping their relative concentrations the same. We calculate the rejection of boron [see Fig. 5(b)] and interestingly, for the current value of membrane charge, boron rejection is almost at a maximum, which we locate at $\alpha = 1.5$ to be $R_B = 93.6\%$. Even reducing membrane charge dramatically, there is not much of a reduction in the ability of the membrane to reject boron, with $R_B = 92\%$ at a 100 times reduced membrane charge. The independence of boron retention on membrane charge can be explained by the fact that the neutral boron in the form of boric acid passes the membrane while not being affected by charge. For all values of α considered, salt rejection remains very high, at values above 99.5%.

Calculation results for different values of pH of seawater (keeping the total carbonate concentration the same) are that for a 50× reduced membrane charge R_B is not affected much by $p\mathrm{H}_{\mathrm{feed}}$ in the entire range studied of $4 < p\mathrm{H}_{\mathrm{feed}} < 10$ (not shown). However, for the standard value of membrane charge and one with 10× more charge, though R_B is not

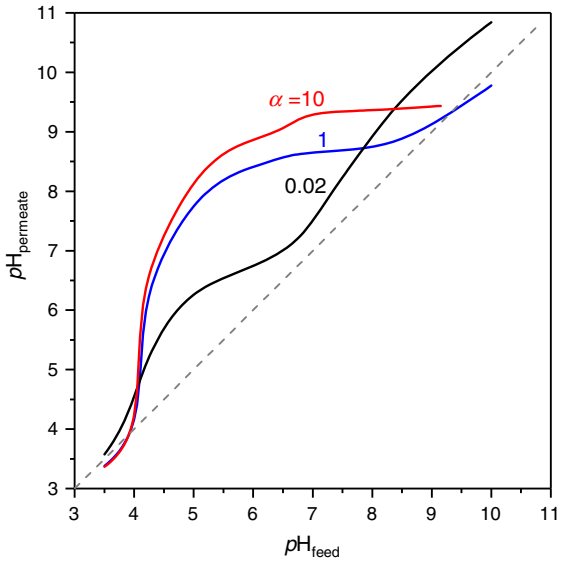

FIG. 10. $p\mathrm{H}_{\mathrm{permeate}}$ as a function of $p\mathrm{H}_{\mathrm{feed}}$ for three different values of the relative membrane charge α, for conditions of Table II, $v_f = 10\ \mu\mathrm{m/s}$.

changed for $p\mathrm{H}_{\mathrm{feed}}$ less than 8.0, for $p\mathrm{H}_{\mathrm{feed}}$ beyond 8.0, boron rejection goes up significantly, up to 99% at $p\mathrm{H}_{\mathrm{feed}} = 10$. Though this calculation result is interesting, it is probably not of much practical relevance because increasing the pH of seawater will lead to severe scaling of the system.

Finally, we present our results for the effect of $p\mathrm{H}_{\mathrm{feed}}$ on $p\mathrm{H}_{\mathrm{permeate}}$ for three different values of membrane charge (Fig. 10). Except for very extreme $p\mathrm{H}_{\mathrm{feed}}$, in all cases $p\mathrm{H}_{\mathrm{permeate}}$ is higher than $p\mathrm{H}_{\mathrm{feed}}$. For $p\mathrm{H}_{\mathrm{feed}} \sim 8.0$, the increase is around 1 pH point, but this increase is less at higher $p\mathrm{H}_{\mathrm{feed}}$. For lower $p\mathrm{H}_{\mathrm{feed}}$, down to pH 4, for the membranes with the original charge or larger, permeate pH can be higher by around 3 pH points, while for the (almost) uncharged membrane, effluent pH is not more than 1 pH point higher than that of the feed. Our calculation results can also be compared to two literature sources with experimental data. For the standard value of membrane charge ($\alpha = 1$), the measurements for seawater reverse osmosis are well reproduced by our model: for $p\mathrm{H}_{\mathrm{feed}} = 8.0$, we predict $p\mathrm{H}_{\mathrm{permeate}} = 8.75$, while experimentally a value of $p\mathrm{H}_{\mathrm{permeate}} = 8.6$–$8.8$ is reported [66], and for $p\mathrm{H}_{\mathrm{feed}} = 9.0$, we predict $p\mathrm{H}_{\mathrm{permeate}} = 9.1$, while the experimental value is $p\mathrm{H}_{\mathrm{permeate}} = 9.1$–$9.5$ [67].

V. CONCLUSIONS

In this work, we develop and apply a theoretical transport model to describe the desalination of seawater using a membrane with a very thin polyamide top layer. The feed water is chosen to mimic seawater and, thus, contains high concentrations of NaCl, which is in contrast to some other theoretical studies which focus on more dilute systems. We investigate the influence of water flow rate (related to applied pressure), membrane charge, and seawater pH. The water equilibrium and two weak acid systems—boric and carbonic acid—are considered additionally to the major ionic constituents. In the model, the membrane is described as a tortuous-porous polymeric structure that holds a fixed amount of pH-dependent charge. The transport in the membrane is described by a Maxwell-Stefan approach including three driving forces contributing to transport: diffusion, migration, and advection. Ions are considered to travel through the membrane while retaining their hydration shell, except for carbonate and bicarbonate for which we assume a reduction in the hydrated size to make them fit into the pores. The ion distribution at the membrane-solution interfaces considers the partitioning factor which is based on the size of the ions. Hindered transport of the ions in the pores of the membrane is accounted for by hydrodynamic correction factors, one for diffusion and migration and one for convection.

The model shows that, in general, diffusion is the dominant driving force for the transport of ions in the membrane, while as the water velocity increases, ion concentration profiles become steeper. For all fluid velocities, pH is lower in the membrane than in the feed, but on the permeate side, it is higher than feed pH. An increase in membrane charge does not improve boron rejection, but a lower membrane charge increases permeate pH, which might be helpful if second-stage RO is employed for boron removal. Neither changes in pH nor membrane charge affect salt rejection significantly, which always remains above 99%.

ACKNOWLEDGMENTS

This work was performed in the cooperation framework of Wetsus, European Centre of Excellence for Sustainable Water Technology. Wetsus is cofunded by the Dutch Ministry of Economic Affairs and Ministry of Infrastructure and Environment, the Province of Fryslân, and the Northern Netherlands Provinces.

[1] UN-Water Thematic Initiatives, Coping with water scarcity: A strategic issue and priority for system-wide action, 2006, http://www.unwater.org/publications/coping-water-scarcity/.
[2] A. A. Burbano, S. S. Adham, and W. R. Pearce, The state of full-scale RO/NF desalination—Results from a worldwide survey, J. Am. Water Works Assoc. **99**, 116 (2007).
[3] R. W. Baker, *Membrane Technology and Applications* (Wiley, New York, 2004).
[4] R. Larson, J. Cadotte, and R. Petersen, The FT-30 seawater reverse osmosis membrane–Element test results, Desalination **38**, 473 (1981).
[5] M. Elimelech and W. A. Phillip, The future of seawater desalination: Energy, technology, and the environment, Science **333**, 712 (2011).

[6] L. Malaeb and G. M. Ayoub, Reverse osmosis technology for water treatment: State of the art review, Desalination **267**, 1 (2011).

[7] J. Palmeri and X. Lefebvre, in *Handbook of Theoretical and Computational Nanotechnology*, edited by M. Rieth and W. Schommers (American Scientific Publishers, Valencia, 2006), Vol. 5, pp. 93–214.

[8] S. Bason, Y. Oren, and V. Freger, Ion transport in the polyamide layer of RO membranes: Composite membranes and free-standing films, J. Membr. Sci. **367**, 119 (2011).

[9] O. Nir, N. F. Bishop, O. Lahav, and V. Freger, Modeling *p*H variation in reverse osmosis, Water Res. **87**, 328 (2015).

[10] J. G. Wijmans and R. W. Baker, The solution-diffusion model—A review, J. Membr. Sci. **107**, 1 (1995).

[11] M. Shen, S. Keten, and R. M. Lueptow, Dynamics of water and solute transport in polymeric reverse osmosis membranes via molecular dynamics simulations, J. Membr. Sci. **506**, 95 (2016).

[12] S. Loeb and S. Sourirajan, Sea water demineralization by means of an osmotic membrane, Adv. Chem. Ser. **38**, 117 (1963).

[13] K. P. Lee, T. C. Arnot, and D. Mattia, A review of reverse osmosis membrane materials for desalination-development to date and future potential, J. Membr. Sci. **370**, 1 (2011).

[14] D. Li and H. Wang, Recent developments in reverse osmosis desalination membranes, J. Mater. Chem. **20**, 4551 (2010).

[15] W. T. Bates, Reducing the fouling rate of surface and waste water RO systems, International Water Conference (1998), http://www.bigbrandwater.com/assets/library/hydranautics/hydranautics-reducing-fouling-ro.pdf.

[16] B. D. Zdravkov, J. J. Cermák, M. Sefara, and J. Janků, Pore classification in the characterization of porous materials: A perspective, Cent. Eur. J. Chem. **5**, 1158 (2007).

[17] R. J. Petersen, Composite reverse osmosis and nanofiltration membranes, J. Membr. Sci. **83**, 81 (1993).

[18] A. K. Ghosh, B. H. Jeong, X. Huang, and E. M. V. Hoek, Impacts of reaction and curing conditions on polyamide composite reverse osmosis membrane properties, J. Membr. Sci. **311**, 34 (2008).

[19] S. H. Lee and J. C. Rasaiah, Proton transfer and the mobilities of the H and OH ions from studies of a dissociating model for water, J. Chem. Phys. **135**, 124505 (2011).

[20] K. Košutić, D. Dolar, and B. Kunst, On experimental parameters characterizing the reverse osmosis and nanofiltration membranes' active layer, J. Membr. Sci. **282**, 109 (2006).

[21] K. Kezia, J. Lee, A. J. Hill, and S. E. Kentish, Convective transport of boron through a brackish water reverse osmosis membrane, J. Membr. Sci. **445**, 160 (2013).

[22] Y. Yoon and R. M. Lueptow, Removal of organic contaminants by RO and NF membranes, J. Membr. Sci. **261**, 76 (2005).

[23] S. Kim and E. M. V. Hoek, Modeling concentration polarization in reverse osmosis processes, Desalination **186**, 111 (2005).

[24] O. Coronell, B. J. Mari nas, X. Zhang, and D. G. Cahill, Quantification of functional groups and modeling of their ionization behavior in the active layer of FT30 reverse osmosis membrane, Environ. Sci. Technol. **42**, 5260 (2008).

[25] A. Bennett, Desalination: 50 years of progress, Filtr. Sep. **50**, 32 (2013).

[26] C. Fritzmann, J. Löwenberg, T. Wintgens, and T. Melin, State-of-the-art of reverse osmosis desalination, Desalination **216**, 1 (2007).

[27] The Dow Chemical Company, Water chemistry and pretreatment: Feedwater type and analysis, 2017, http://msdssearch.dow.com/PublishedLiteratureDOWCOM/dh_003b/0901b8038003b48d.pdf.

[28] D. Dyrssen and I. Hansson, Ionic medium effects in sea water—A comparison of acidity constants of carbonic acid and boric acid in sodium chloride and synthetic sea water, Mar. Chem. **1**, 137 (1973).

[29] A. G. Dickson and J. P. Riley, The estimation of acid dissociation constant in seawater media from potentiometric titrations with strong base, Mar. Chem. **7**, 89 (1979).

[30] R. E. Zeebe, A. Sanyal, J. D. Ortiz, and D. A. Wolf-Gladrow, A theoretical study of the kinetics of the boric acid-borate equilibrium in seawater, Mar. Chem. **73**, 113 (2001).

[31] K. L. Tu, L. D. Nghiem, and A. R. Chivas, Boron removal by reverse osmosis membranes in seawater desalination applications, Sep. Purif. Technol. **75**, 87 (2010).

[32] E. Mastromatteo and F. Sullivan, Summary: International symposium on the health effects of boron and its compounds, Environ. Health Perspect. **102**, 139 (1994).

[33] T. A. Devirian and S. L. Volpe, The physiological effects of dietary boron, Crit. Rev. Food Sci. Nutr. **43**, 219 (2003).

[34] T. L. Litovitz, W. Klein-Schwartz, G. M. Oderda, and B. F. Schmitz, Clinical manifestations of toxicity in a series of 784 boric acid ingestions, Am. J. Emerg. Med. **6**, 209 (1988).

[35] C. H. Linden, A. H. Hall, K. W. Kulig, and B. H. Rumack, Acute ingestions of boric acid, J. Toxicol. Clin. Toxicol. **24**, 269 (1986).

[36] World Health Organization, *Guidelines for Drinking-Water Quality*, 4th ed. (2011), http://www.who.int/water_sanitation_health/publications/dwq-guidelines-4/en/.

[37] S. H. Frisbie, E. J. Mitchell, and B. Sarkar, Urgent need to reevaluate the latest World Health Organization guidelines for toxic inorganic substances in drinking water, Environ. Health **14**, 63 (2015).

[38] R. S. Ayers and D. W. Westcot, Water quality for agriculture, *Food and Agricultural Organization*, 1985, p. 97, http://www.fao.org/docrep/003/T0234E/T0234E00.htm.

[39] H. Corti, R. Crovetto, and R. Fernandez-Prini, Properties of the borate ion in dilute aqueous solutions, J. Chem. Soc., Faraday Trans. 1 **76**, 2179 (1980).

[40] J. R. Werber, A. Deshmukh, and M. Elimelech, The critical need for increased selectivity, not increased water permeability, for desalination membranes, Environ. Sci. Technol. Lett. **3**, 112 (2016).

[41] E. Güler, C. Kaya, N. Kabay, and M. Arda, Boron removal from seawater: State-of-the-art review, Desalination **356**, 85 (2015).

[42] N. Hilal, G. J. Kim, and C. Somerfield, Boron removal from saline water: A comprehensive review, Desalination **273**, 23 (2011).

[43] F. J. Millero, The thermodynamics of the carbonate system in seawater, Geochim. Cosmochim. Acta **43**, 1651 (1979).

[44] A. G. Dickson and F. J. Millero, A comparison of the equilibrium constants for the dissociation of carbonic acid in seawater media, Deep Sea Res. Part A **34**, 1733 (1987).

[45] R. Rautenbach and A. Albrecht, *Membrane Processes* (Wiley, New York, 1989), Chap. 3, pp. 48–74.

[46] E. Spruijt and P. M. Biesheuvel, Sedimentation dynamics and equilibrium profiles in multicomponent mixtures of colloidal particles, J. Phys. Condens. Matter **26**, 075101 (2014).

[47] W. M. Deen, Hindered transport of large molecules in liquid-filled pores, AIChE J. **33**, 1409 (1987).

[48] A. Szymczyk and P. Fievet, Investigating transport properties of nanofiltration membranes by means of a steric, electric and dielectric exclusion model, J. Membr. Sci. **252**, 77 (2005).

[49] H. Brenner and L. J. Gaydos, The constrained Brownian movement of spherical particles in cylindrical pores of comparable radius. Models of the diffusive and convective transport of solute molecules in membranes and porous media, J. Colloid Interface Sci. **58**, 312 (1977).

[50] P. B. Peters, R. Van Roij, M. Z. Bazant, and P. M. Biesheuvel, Analysis of electrolyte transport through charged nanopores, Phys. Rev. E **93**, 053108 (2016).

[51] M. Tedesco, H. V. M. Hamelers, and P. M. Biesheuvel, Nernst-Planck transport theory for (reverse) electrodialysis: II. Effect of water transport through the membranes, J. Membr. Sci. **510**, 370 (2016).

[52] P. M. Biesheuvel, Two-fluid model for the simultaneous flow of colloids and fluids in porous media, J. Colloid Interface Sci. **355**, 389 (2011).

[53] A. A. Sonin, in *Charged Gels and Membranes I*, edited by E. Sélégny (D. Reidel, Dordrecht, 1976), pp. 255–265.

[54] V. Freger, Swelling and morphology of the skin layer of polyamide composite membranes: An atomic force microscopy study, Environ. Sci. Technol. **38**, 3168 (2004).

[55] K. Kezia, J. Lee, W. Ogieglo, A. Hill, N. E. Benes, and S. E. Kentish, The transport of hydronium and hydroxide ions through reverse osmosis membranes, J. Membr. Sci. **459**, 197 (2014).

[56] X. Zhang, D. G. Cahill, O. Coronell, and B. J. Mari nas, Partitioning of salt ions in FT30 reverse osmosis membranes, Appl. Phys. Lett. **91**, 181904 (2007).

[57] H. Koseoglu, N. Kabay, M. Yuksel, S. Sarp, O. Arar, and M. Kitis, Boron removal from seawater using high rejection SWRO membranes-impact of *p*H, feed concentration, pressure, and cross-flow velocity, Desalination **227**, 253 (2008).

[58] Lenntech, Major ion composition of seawater, http://www.lenntech.com/composition-seawater.htm.

[59] E. R. Nightingale, Phenomenological theory of ion solvation. Effective radii of hydrated ions, J. Phys. Chem. **63**, 1381 (1959).

[60] P. Atkins and J. de Paula, *Physical Chemistry*, 9th ed. (Oxford University Press, 2009), pp. 430–468.

[61] E. Goli, T. Hiemstra, W. H. Van Riemsdijk, R. Rahnemaie, and M. J. Malakouti, Diffusion of neutral and ionic species in charged membranes: Boric acid, arsenite, and water, Anal. Chem. **82**, 8438 (2010).

[62] J. E. Dykstra, P. M. Biesheuvel, H. Bruning, and A. Ter Heijne, Theory of ion transport with fast acid-base equilibrations in bioelectrochemical systems, Phys. Rev. E **90**, 013302 (2014).

[63] B. Tansel, Significance of thermodynamic and physical characteristics on permeation of ions during membrane separation: Hydrated radius, hydration free energy and viscous effects, Sep. Purif. Technol. **86**, 119 (2012).

[64] W. R. Bowen, A. W. Mohammad, and N. Hilal, Characterisation of nanofiltration membranes for predictive purposes—Use of salts, uncharged solutes and atomic force microscopy, J. Membr. Sci. **126**, 91 (1997).

[65] S. Bandini and D. Vezzani, Nanofiltration modeling: The role of dielectric exclusion in membrane characterization, Chem. Eng. Sci. **58**, 3303 (2003).

[66] B. Andrews, B. Davé, P. López-Serrano, S.-P. Tsai, R. Frank, M. Wilf, and E. Koutsakos, Effective scale control for seawater RO operating with high feed water *p*H and temperature, Desalination **220**, 295 (2008).

[67] O. Nir, E. Marvin, and O. Lahav, Accurate and self-consistent procedure for determining *p*H in seawater desalination brines and its manifestation in reverse osmosis modeling, Water Res. **64**, 187 (2014).

[68] P. M. Biesheuvel, Thermodynamic cycle analysis for capacitive deionization, J. Colloid Interface Sci. **332**, 258 (2009).

[69] C. Dominguez-Tagle, V. J. Romero-Ternero, and A. M. Delgado-Torres, Boron removal efficiency in small seawater reverse osmosis systems, Desalination **265**, 43 (2011).